Aerosol and Air Quality Research, 20: 193–202, 2020

ISSN: 1680-8584 print / 2071-1409 online
doi: 10.4209/aaqr.2019.09.0467

Plasma-catalytic Oxidation of Toluene on Ag Modified FeO_x/SBA-15

Meijuan Lu[1,2], Wenting Yang[3], Chenglong Yu[1], Qian Liu[4], Daiqi Ye[2*]

[1] *School of Environmental and Land Resource Management, Jiangxi Agricultural University, Nanchang 330045, China*
[2] *College of Environment and Energy, South China University of Technology, Guangzhou 510006, China*
[3] *School of Agricultural Sciences, Jiangxi Agricultural University, Nanchang 330045, China*
[4] *School of Sciences, Jiangxi Agricultural University, Nanchang 330045, China*

ABSTRACT

Catalysts created by loading FeO_x and AgO_x on SBA-15 surfaces via wet impregnation were used to remove toluene with the assistance of non-thermal plasma (NTP). The catalysts were characterized with X-ray diffraction (XRD), scanning electron microscopy (SEM), and H_2 temperature-programmed reduction (H_2-TPR). The results showed that incorporating the SBA-15, 3%FeO_x/SBA-15 and 2%FeO_x–1%AgO_y/SBA-15 catalysts enhanced the toluene removal efficiency and CO_2 selectivity of the NTP system. The silver particles tended to cover the catalyst surface in the form of Ag and Ag_2O, which lengthened the residual time of toluene in the NTP-catalytic system, thereby promoting the reaction of toluene with oxygen on the catalyst surface. Simultaneously, introducing Ag improved the distribution of FeO_x on the catalyst surface, increasing toluene oxidation and catalyst stability. According to our analysis of the toluene removal efficiency, identification of organic byproducts, and in situ FT-IR spectroscopy of the toluene adsorption, FeO_x and AgO_x significantly enhance the efficiency of toluene degradation in plasma-assisted catalytic systems.

Keywords: FeO_x-AgO_y/SBA-15 catalyst; Toluene removal; Plasma-catalytic oxidation.

INTRODUCTION

Non-thermal plasma (NTP) combined catalysis technology is a promising method for VOCs oxidation due to its high economy and energy efficiency (Stasiulaitiene *et al.*, 2016; Lu *et al.*, 2019). At the same time, the FeO_x shows the outstanding performance for toluene removal in the NTP system. However, CO and other byproducts are formed during toluene degradation, and CO_2 selectivity is low (Lu *et al.*, 2015). In order to overcome these disadvantages, the catalysts of bimetallic materials have been applied for VOCs degradation due to their prominent catalytic activity (Jiang *et al.*, 2016; Zhu *et al.*, 2016; Jiang *et al.*, 2019). Noble-metal-based catalysts, such as Pt, Au, are traditional catalysts for the VOCs oxidation at low temperatures (Li *et al.*, 2016; Yang *et al.*, 2016). However, these pure noble metal catalysts also have some disadvantages, especially their high cost. Scirè *et al.* (2001) report that Ag could weaken the Fe-O bond, increase the mobility of the lattice oxygen, and thus improve the VOCs oxidation. Meanwhile, Ag has exceptional activity and is more economical (Jiang *et al.*, 2016; Pangilinan *et al.*, 2016). In addition, Ag could work as an adsorption center, improving adsorption ability and oxidation for VOCs (Chen *et al.*, 2011; Huang *et al.*, 2015). However, there has been little research in regards to combining this bimetallic oxide catalyst with NTP for VOCs degradation in the present literatures. Besides that, the effect of bimetallic catalyst on VOCs degradation in NTP system is still not clear. Therefore, we incorporated Ag into the FeO_x catalyst on account of the characteristics of these two materials, and co-loaded them on the surface of SBA-15 which has uniform mesoporous channels, high specific surface area, and high adsorption ability for toluene (Zhang *et al.*, 2012b; Qin *et al.*, 2019).

In this work, toluene was selected as the targeted pollutant, and the plasma-catalytic oxidization was carried out at identical specific energy density (SIE) under the condition of atmospheric pressure and room temperature. In order to study the structure and possible interaction between FeO_x and AgO_y species, the catalysts were characterized by XRD, SEM and H_2-TPR. In situ FT-IR spectroscopy of toluene adsorption and organic byproducts on catalyst surface were also identified to acquire the toluene oxidation mechanism on the surface of FeO_x-AgO_y/SBA-15 catalyst.

EXPERIMENT

Experimental Setup

The schematic diagram of the experimental setup is

* Corresponding author.
Tel.: +86 20 39380516; Fax: +86 20 39380518
E-mail address: cedqye@scut.edu.cn

shown in Fig. 1. The toluene was obtained by bubbling liquid toluene with an N_2 gas stream in a bubbler, which was described in our previous study (Lu *et al.*, 2015). Then, the reaction gas was introduced into the reactor with an initial toluene concentration of 100 ppm at a flow rate of 180 mL min^{-1}. The initial toluene concentration and the gas flow rate were adjusted by mass flow controllers (MFCs) (Seven Star Co., China).

Toluene oxidation was carried out in a fixed-bed flow reactor containing 0.12 g of the catalyst (40–60 mesh) and 0.96 g of silica sand (40–60 mesh). The outgoing gas was analyzed using an online gas chromatograph (GC2014C; Shimadzu) equipped with two FID detectors: one for organic compounds, featuring a TG-BOND Q column (30 m, 0.32 mm; 60°C), and the other, equipped with a methanizer, for carbon monoxide and carbon dioxide analysis using a 5 A molecular sieve (2 m, 2 mm) and PoraPLOT Q column (4 m, 2 mm) (60°C). The toluene removal efficiency and CO_2 selectivity were calculated based on the following formulas:

$$\text{Toluene removal efficiency (\%)} = \frac{C_{in} - C_{out}}{C_{in}} \times 100\% \quad (1)$$

$$CO_2 \text{ selectivity (\%)} = \frac{C_{CO_2}}{7(C_{in} - C_{out})} \times 100\% \quad (2)$$

where C_{in} and C_{out} are the inlet and outlet toluene concentrations respectively, C_{CO_2} is the outlet concentration of CO_2. All concentrations were measured in ppm, and the data was recorded by an online gas chromatograph when the toluene removal efficiency was stabilized.

Plasma System

The reactor was a cylinder reactor of quartz glass, with an inner diameter of 8 mm and wall thickness of 1 mm. The stainless steel wire mesh was wrapped as the ground electrode, and a stainless steel rod (o.d. = 2 mm) was used as the inner electrode, resulting in the discharge length and discharge gap being 18 mm and 3 mm. The reactor was powered by an AC high-voltage power supplying with the frequency of 2 kHz (CTP-2000k; Corona Laboratory, Nanjing, China). In the experiment, the discharge power was measured by the areas of the voltage-charge Lissajous figures, which were acquired by an oscilloscope (TDS1002; Tektronix) (Li *et al.*, 2014).

The specific energy density (SED) was calculated from the following expression:

$$\text{SED}\left(\text{J L}^{-1}\right) = \frac{\text{Discharge power (W)}}{\text{Gas flow rate (L s}^{-1})} \quad (3)$$

Catalyst Preparation and Characterization

The catalysts were prepared using wetness impregnation method. Iron nitrate ethanol solution (Fe/SBA-15 = 2% wt. and 3% wt.) was first added to SBA-15 powder, after being stirred at room temperature for 24 h, the solvent was then removed by evaporation at 60°C. The residue was dried at 120°C for 12 h, calcined at 500°C for 4 h. The resulting catalysts were denoted as 2%FeO_x/SBA-15, 3%FeO_x/SBA-15, respectively. After that, Ag was loaded on the catalyst of 2%FeO_x/SBA-15 using a similar process under the same condition with $AgNO_3$ solutions as precursors (Ag/SBA-15 = 1% wt.). The resulting catalyst was denoted as 2%FeO_x–1%AgO_y/SBA-15.

XRD results were collected using a D8 ADVANCE X-ray diffractometer (Bruker, Germany) operated at 40 kV and 40 mA using Ni-filtered Cu Kα radiation, the 2θ ranges were 0.6–5° and 5–90° at a scanning rate of 4° min^{-1}.

SEM microphotographs were collected with an S-3700N electron microscope (Hitachi, Japan) operating at 5.0 kV. H_2-TPR data was collected by a Micromeritics AutoChem II 2920 instrument. Each catalyst (40 mg) was pretreated at 300°C in the high-purity Ar (30 mL min^{-1}) for 30 min and then cooled to 60°C. Subsequently, the flow of an H_2-Ar

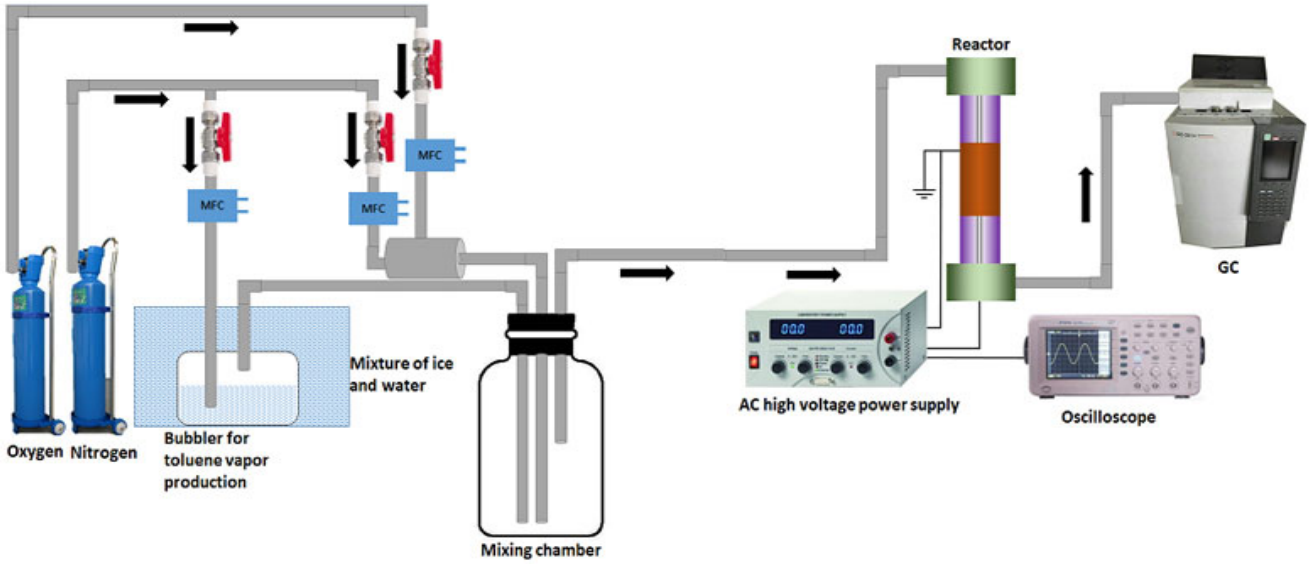

Fig. 1. Schematic illustration of the experimental setup.

mixture (10% H_2 by volume) was switched on, and the catalyst was heated to 700°C at a rate of 10°C min^{-1}. The H_2 consumption was monitored by a thermal conductivity detector (TCD).

In Situ FT-IR Study

In situ FT-IR spectra was recorded using a Nicolet 6700 spectrometer equipped with a mercury-cadmium-telluride (MCT) detector cooled by liquid nitrogen. The catalyst was pretreated at 300°C in high-purity Ar (100 mL min^{-1}) for 60 min, cooled to room temperature, then toluene–N_2-O_2 mixture (100 ppm toluene, N_2:O_2 = 20%:80%) was introduced into the IR cell. The infrared spectra of toluene adsorption were collected with a resolution of 2 cm^{-1} and 64 scans in the region of 650–4000 cm^{-1}.

Identification of Organic Byproducts on the Catalyst Surface

The organic byproducts on the catalyst surface were extracted by CS_2 solution (chromatographic grade) at the condition of ultrasonic vibration for 120 min. Then filtered with a 0.22 μm filter membrane, and analyzed by a GC–MS (QP2010; Shimadzu) with Rtx-5MS capillary column. The column temperature was firstly maintained at 40°C for 2 min, then increased to 220°C with a rate of 6°C min^{-1}, and maintaining for 5 min. MS identification was conducted using the NIST 08 databank (NIST/EPA/NIH Mass Spectral Library).

RESULTS AND DISCUSSION

Catalytic Activity Evaluation

The results of toluene removal efficiency and CO_2 selectivity were showed in Fig. 2. The toluene removal efficiency was only 47% under the condition of NTP, while it significantly increased as the various catalysts were packed into the plasma system. The toluene removal efficiency caused by SBA-15, 3%FeO_x/SBA-15, 2%FeO_x–1%AgO_y/SBA-15 increased by 48.9%, 50.3%, 51.3% respectively. CO_2 selectivity had no significant change over the SBA-15, while it was increased by 11% over the 3%FeO_x/SBA-15 and 17% over the 2%FeO_x–1%AgO_y/SBA-15 catalyst. This suggests that the catalytic activity of composite metal oxides is higher than that of single component. In view of the reason, Wang *et al.* (2015) and Chen *et al.* (2011) found that the catalysts loaded with Ag could form stronger π-complex and had higher adsorption capacity for toluene, resulting remain time in the plasma system was increased. Ag could also weaken the Fe-O bond and increase the lattice oxygen mobility (Scirè *et al.*, 2001). On the other hand, Ag reoxidation was readily accomplished by the transfer of adsorbed oxygen from FeO_x, which could contribute to maintain the good performance for toluene degradation in the plasma system. These results indicate that the interaction between Ag and Fe species could increase the catalyst activity, and consequently improve the performance of the plasma-catalytic degradation of toluene.

In Situ FT-IR Spectroscopy of Toluene Adsorption

In situ FT-IR technology could provide continuous monitoring for VOCs adsorption over the catalyst surface (Augugliaro *et al.*, 1999). Therefore, in situ FT-IR spectroscopy of toluene adsorption over the catalyst surface was carried out under the condition of 80% N_2 + 20% O_2 (Fig. 3). The band of the toluene adsorption appeared on all the catalysts: 1392, 1460, 1495 and 1608 cm^{-1} characteristics of aromatic ring C=C stretching vibration (Li *et al.*, 2007); 2879, 2928 cm^{-1} characteristics of C-H vibrations of methyl (Maira *et al.*, 2001; Eby *et al.*, 2012); 3031 cm^{-1} characteristic of C-H vibration of aromatic ring (Maira *et al.*, 2001). Also, the new adsorption bands at 1120, assigned to terpene OH stretching (Das *et al.*, 2014), and 1167, assigned to ester C-O stretching (Long *et al.*, 2011; Yang *et al.*, 2013), appeared on the surface of catalyst loaded with Ag. This indicates that the toluene oxidation on the catalyst surface was improved due to the Ag introduction. However, deep oxidization was not accomplished at room temperature, and as a result, it

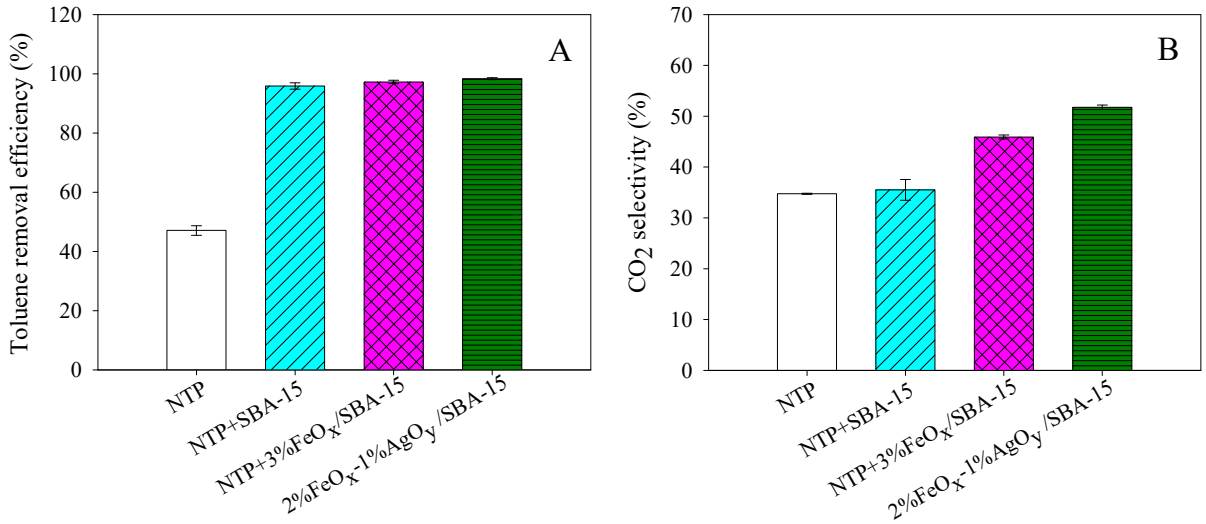

Fig. 2. Effect of catalyst on (A) toluene removal efficiency and (B) CO_2 selectivity (Initial concentration of toluene: 100 ppm, SED: 767 J L^{-1}).

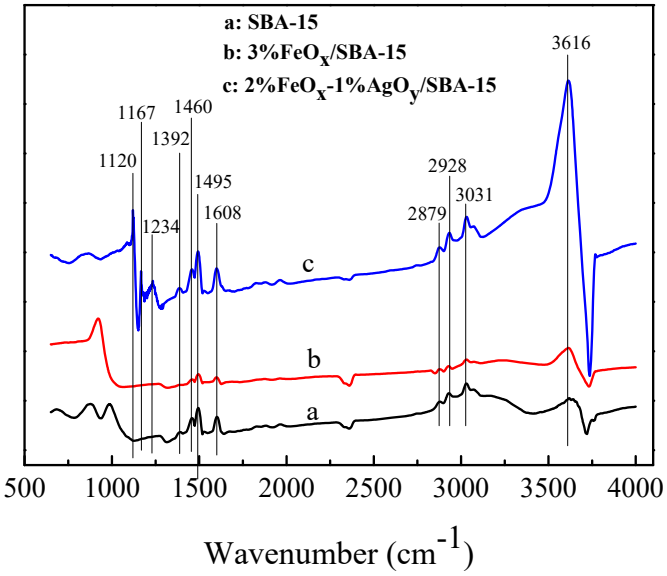

Fig. 3. In situ FT-IR spectroscopy of toluene adsorption over the catalyst surface (Initial concentration of toluene: 100 ppm, background gas: 80%N_2 + 20%O_2).

produced unexpected terpenoid and ester. There was no significant difference for the absorption band at 3616 cm^{-1}, characteristic ascribed to OH stretching (Li *et al.*, 2011a, b), on the SBA-15 and 3%FeO_x/SBA-15, while this peak intensity increased on the surface of 2%FeO_x–1%AgO_y/SBA-15 catalyst. Those indicate that Ag incorporation could promote the generation of derivatives related to OH (Li *et al.*, 2011b), which might be beneficial to toluene degradation on the surface of catalyst (Fig. 2).

Analysis of the Toluene Oxidation Residues

Byproducts on the catalyst surface were monitored by GC-MS (Fig. 4). The results show that the benzaldehyde, 4-methyl-2-pentanone had relatively high amounts on the SBA-15 surface, while they significantly decreased when Fe and Ag were introduced. This suggests that Fe and Ag loading could promote toluene oxidation in the process of NTP combined catalyst, which agreed with the results of CO_2 selectivity (Fig. 2).

Catalyst Characterization

In order to study the relationship between catalyst structure and toluene removal efficiency, the catalysts were characterized by XRD (Fig. 5), SEM (Fig. 6) and H_2-TPR (Fig. 7).

XRD

The results of low-angle XRD patterns (Fig. 5(a)) show the characteristic peaks, (100), (110), and (200), of mesoporous material and indicates that highly ordered 2D-hexagonal mesoporous structure of SBA-15 was retained after loading Fe and Ag. Fig. 5(b) shows the wide-angle XRD patterns of SBA-15, 3%FeO_x/SBA-15 and 2%FeO_x–1%AgO_y/SBA-15 catalysts. The Fe_2O_3 and Fe_3O_4 diffraction peaks were clearly observed when 3%Fe was loaded on SBA-15. However, they disappeared while Ag_2O and Ag diffraction peaks were observed as Ag species incorporation. This tendency might be caused by the formation of amorphous iron, or the fact that the particles of iron oxidation are highly dispersed on the support material with the such low amount Fe loading, resulting in the exceedance of detection limit with XRD.

Ag could serve as a reservoir for gas-phase toluene because of the π bond formation with toluene (Huang *et al.*, 2015). Ag^+ is better at adsorbing toluene and weakening its C=C bond (Trinh *et al.*, 2015; Qin *et al.*, 2016). This could promote the toluene transformation from gas phase to the catalyst surface, then decrease the toluene degradation in the gas phase by the NTP, and improve the CO_2 selectivity during the toluene plasma-catalyst oxidation (Fig. 2). In addition, the Ag^+ on the catalyst is essential for high catalytic activity of CO oxidation (Zhang *et al.*, 2013), which might be the reason for high CO_2 selectivity in the process of toluene degradation in the combined Ag-Fe NTP system.

SEM

The catalyst morphology was observed by SEM (Fig. 6). Some small granules appeared and evenly dispersed on the SBA-15 surface when the 3%Fe was loaded. However, the amount of particles decreased as 1%Ag incorporating, and the particles were smaller than those on the surface of 3%FeO_x/SBA-15. In order to study the morphology of the particles on the 2%FeO_x–1%AgO_y/SBA-15 surface, SEM of 2.5%FeO_x–0.5%AgO_y/SBA-15 and 1.5%FeO_x–1.5%AgO_y/SBA-15 were also provided (Figs. 6(d) and 6(e)). There were no large particles on the 2.5%FeO_x–0.5%AgO_y/SBA-15 catalyst, but some particles newly appeared on the 1.5%FeO_x–1.5%AgO_y/SBA-15 surface, and their size was even larger than those on the 3%FeO_x/SBA-15. This suggests that the particles on the 2%FeO_x–1%AgO_y/SBA-15 surface were the Ag compounds, and the diffusion of FeO_x particles were promoted by Ag incorporating. These results might benefit for the improvement of FeO_x catalytic activity.

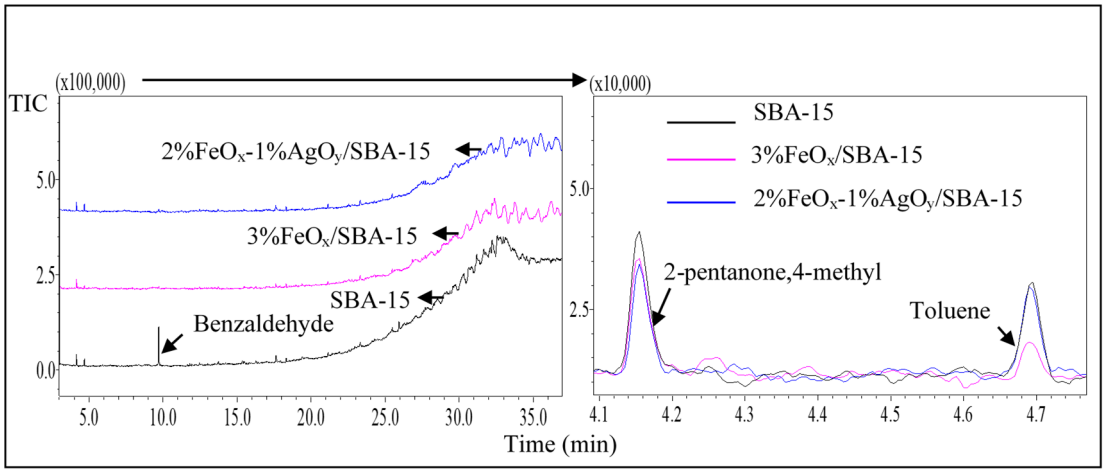

Fig. 4. GC-MS spectrum of organic by-products from toluene decomposition on the catalyst surface.

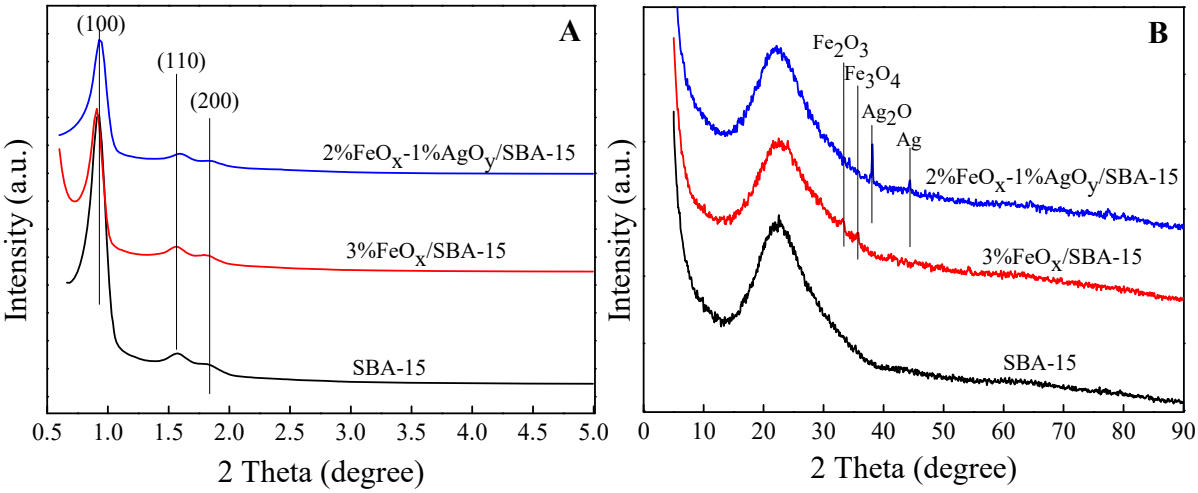

Fig. 5. (A) Low-angle, (B) wide-angle XRD patterns of catalysts.

H_2-TPR

The catalytic property of catalyst was determined by the reducibility, which could be measured by H_2-TPR (Gogoi *et al.*, 2020). Fig. 7 presents the H_2-TPR profiles of different catalysts. The reduction peak at 126°C was observed in all catalysts and had no obvious change after Fe and Ag incorporation, which was attributed to the H_2 consumption by SBA-15. For the 3%FeO_x/SBA-15 catalyst, the low-temperature reduction peak (325°C) and a shoulder peak (438°C) could be attributed to the reduction of $Fe_2O_3 \rightarrow Fe_3O_4 \rightarrow Fe$ (Long *et al.*, 2011; Zhang *et al.*, 2012a). In order to study the reduction of Ag, H_2-TPR profile of 3%AgO_y/SBA-15 was also carried out. Only one reduction peak could be observed at 110°C assigned to the reduction of Ag^+ to Ag (Chen *et al.*, 2011), while it did not appear on others catalysts. Therefore, all the reduction peaks in the 2%FeO_x–1%AgO_y/SBA-15 could be assigned to the reduction of FeO_x. At the same time, all reduction peaks shifted to the lower temperature at the catalyst of 2%FeO_x–1%AgO_y/SBA-15 than 3%FeO_x/SBA-15. This suggests that the reducibility of FeO_x was promoted, indicating that the lattice oxygen mobility was higher in 2%FeO_x–1%AgO_y/SBA-15 (Jin *et al.*, 2013). Therefore, 2%FeO_x–1%AgO_y/SBA-15 catalyst showed the better performance for CO_2 selectivity in the plasma system (Fig. 2(b)).

Pathways of Toluene Degradation

Based on the results of toluene removal efficiency, analysis of organic byproducts, and in situ FT-IR spectroscopy of toluene adsorption, the mechanism of toluene degradation is proposed (Fig. 8). Toluene decomposition in plasma-assisted catalysis could be described to direct plasma reaction and plasma-catalytic surface reaction.

For the direct plasma reaction, it contains direct electron attack or indirect reactions between VOC molecules and gas-phase radicals. As we all know, there are a large number of high-energy electrons in the plasma system, which could react with O_2, H_2O and N_2 in the outlet gas as follows (R4–R10), and form gas-phase radicals (O·, OH· and N_2*) (Blin-Simiand *et al.*, 2009; Yu *et al.*, 2010; Abdelaziz *et al.*, 2013; Liang *et al.*, 2013; Chung *et al.*, 2019). The high-energy electron and the activity radical could induce the toluene degradation (ring opening, oxidation) in gas phase, and formed CO_2 and H_2O.

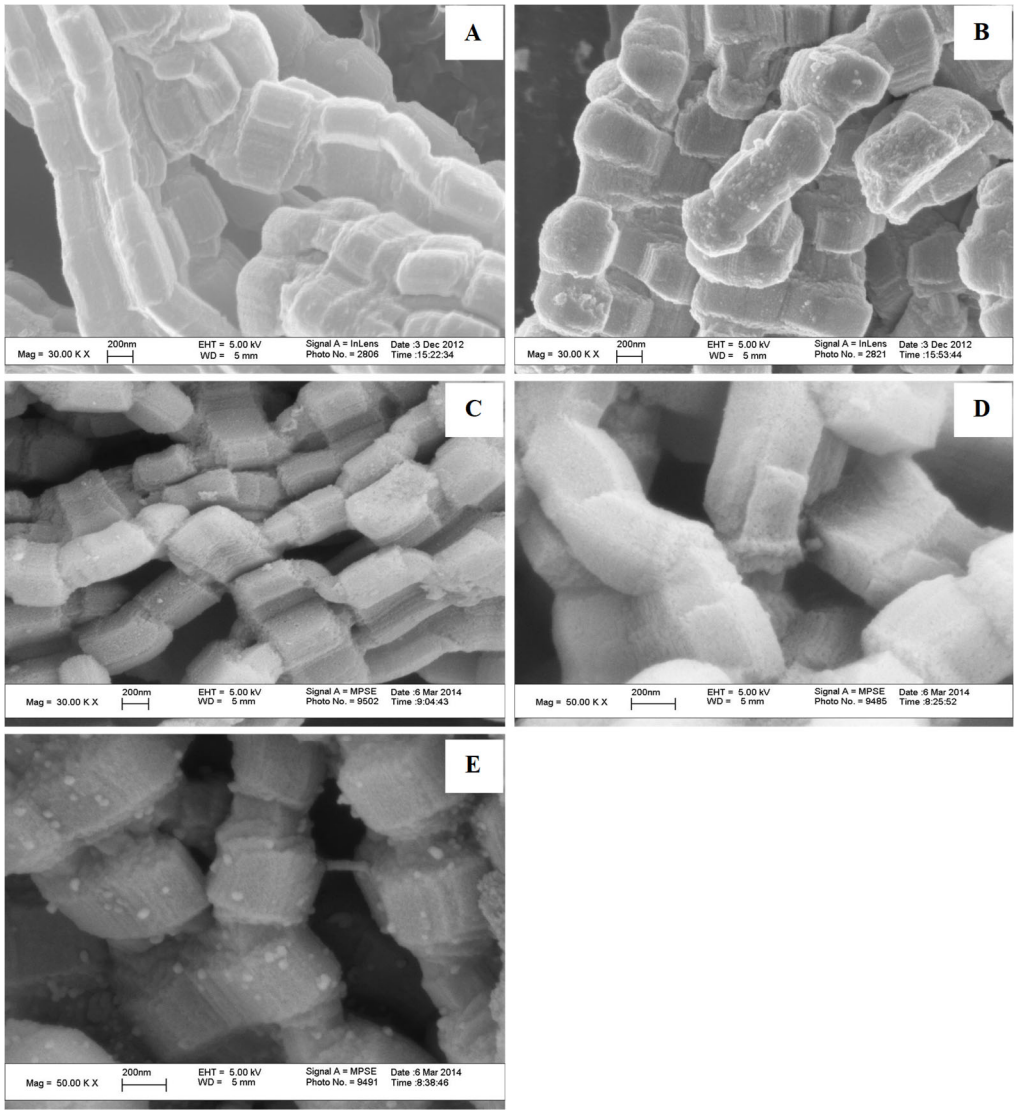

Fig. 6. SEM images of various catalysts. (A) SBA-15, (B) 3%FeO_x/SBA-15, (C) 2%FeO_x–1%AgO_y/SBA-15, (D) 2.5%FeO_x–0.5%AgO_y/SBA-15, (E) 1.5%FeO_x–1.5AgO_y/SBA-15.

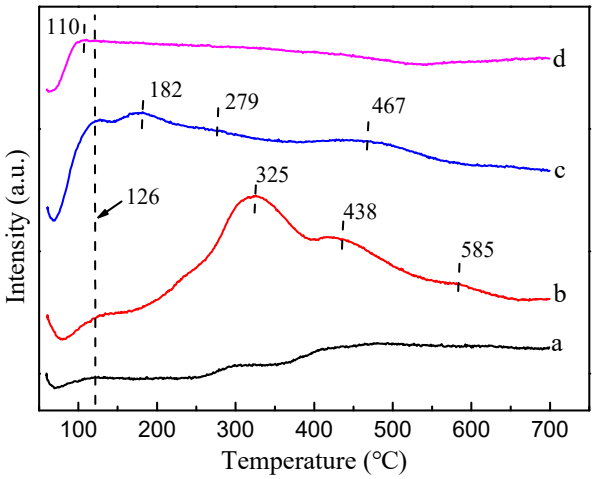

Fig. 7. H_2-TPR profiles of different Fe and Ag loading catalysts (a: SBA-15, b: 3%FeO_x/SBA-15, c: 2%FeO_x–1%AgO_y/SBA-15, d: 3%AgO_y/SBA-15).

$$e + O_2 \rightarrow e + O\cdot(^3P) + O\cdot(^3P) \quad (R4)$$

$$e + O_2 \rightarrow e + O\cdot(^1D) + O\cdot(^1D) \quad (R5)$$

$$e + H_2O \rightarrow OH\cdot + H\cdot \quad (R6)$$

$$e + H_2O \rightarrow O\cdot + 2H\cdot \quad (R7)$$

$$H_2O + O\cdot(^1D) \rightarrow 2OH\cdot \quad (R8)$$

$$N_2 + e \rightarrow N_2^* + e \quad (R9)$$

$$N_2^* + O_2 \rightarrow O(^3P) + O(^3P) + N_2 \quad (R10)$$

When the SAB-15 was introduced into the plasma system, toluene could be adsorbed on the catalyst surface, and oxidized into the benzaldehyde, then experienced through an opening of aromatic ring to form 4-methyl-2-pentanone, and further oxidized into CO_2 and H_2O by O· and ·OH. As the

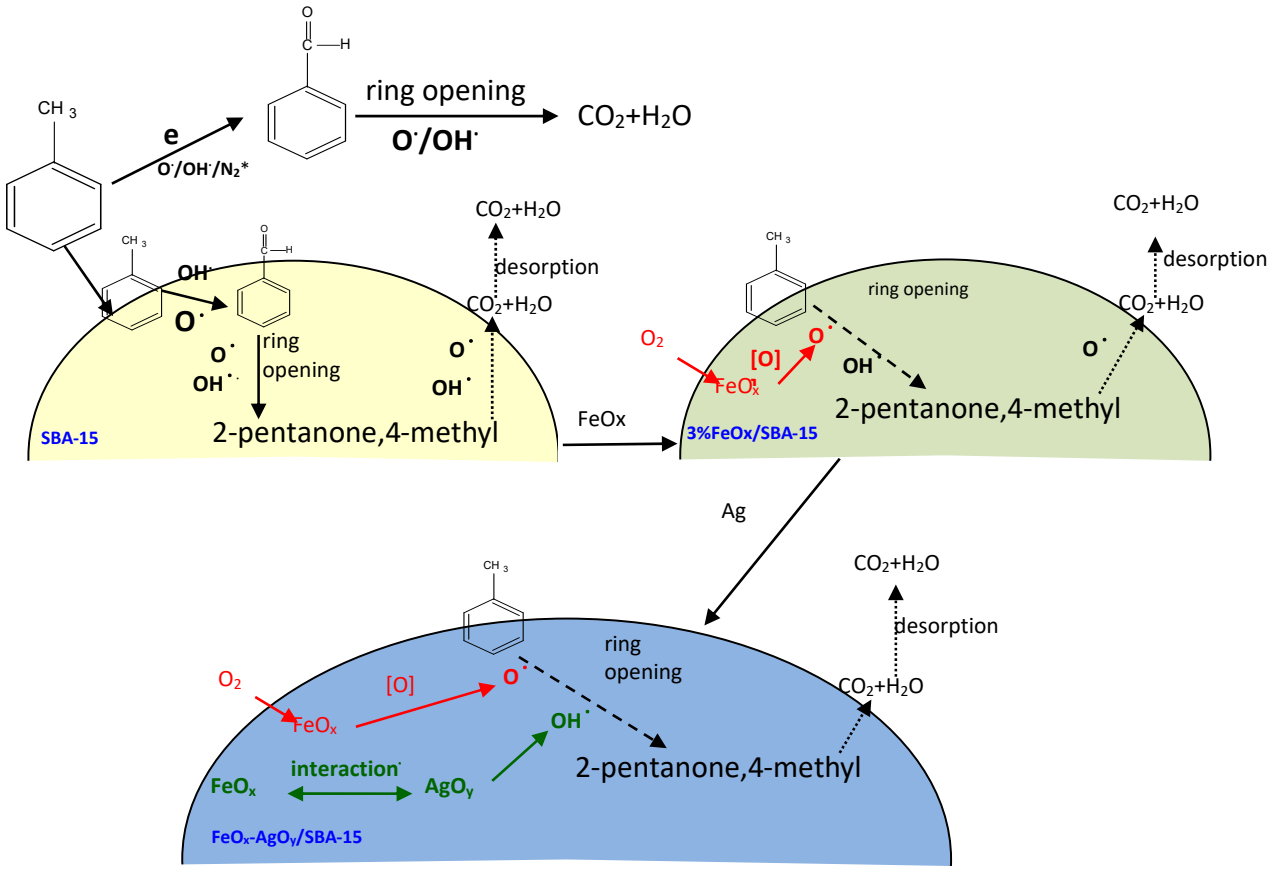

Fig. 8. Pathway of toluene degradation in the plasma-assisted catalyst system.

3%Fe was loaded on the SBA-15 surface, the O_2 in the gas phase could also be adsorbed on the catalyst surface via facile inter-conversion between Fe^{2+} and Fe^{3+} states, which could lead to the formation of free radical of O·. The generated O· was then transported to the toluene on the catalyst surface, leading to a fast opening of its aromatic ring, and the further oxidization to CO_2 which finally desorbed from catalyst surface into gas phase. When Ag was incorporated, the amount of the ·OH was significantly improved (Fig. 3) because of the interaction between FeO_x and AgO_y. As discussed above, a fast opening of the aromatic ring happened and led to the formation 4-methyl-2-pentanone, which then was mineralized to CO_2, and finally desorbed from catalyst surface into gas phase. On the other hand, toluene could also be adsorbed on the catalyst surface because of the π bond formation between Ag and toluene, then oxidized by oxygen from FeO_x adsorbed, subsequently, mineralized into the CO_2 and H_2O. At the same time, Ag reoxidation was readily accomplished by the transfer of adsorbed oxygen from FeO_x. Therefore, the reaction of toluene oxidation could be sustained. Meanwhile, the consumed oxygen species on the catalysts could be replenished by either gas-phase oxygen, or active oxygen species generated during the plasma process. The consumed oxygen in the gas phase would alleviate the effect of oxygen's negative electrons on the process of toluene removal.

Evaluation of Catalyst Stability

The stability of SBA-15, 3%FeO_x/SBA-15 and 2%FeO_x–1%AgO_y/SBA-15 catalysts (Fig. 9), during toluene plasma-catalytic oxidation, was assessed at room temperature and atmospheric pressure. It was observed that toluene removal proceeded stably during the first 19 h for all the catalysts. After that, the toluene removal efficiency decreased in SBA-15 and 3%FeO_x/SBA-15, while the 2%FeO_x–1%AgO_y/SBA-15 catalyst was perfectly stabilized over the period of 37 h for toluene conversion. This suggests that the interaction between Ag and Fe improved the stability of catalyst.

Meanwhile, toluene removal efficiency shows the variation from 80% to 100% in SBA-15 and 3%FeO_x/SBA-15, which might be due to an accumulation of water molecules on the catalyst surface (Lu *et al.*, 2014). However, this phenomenon did not appear at the 2%FeO_x–1%AgO_y/SBA-15 combined NTP system. This suggests that adding Ag improved the catalyst's capability of resisting water molecules, which was very important to improve catalytic activity of the catalyst.

The XRD of the catalysts for different reaction times were compared to study structural stability of the catalysts (Fig. 10). Three characteristic peaks, (100), (110), and (200), characterizing the mesoporous material with 2D-hexagonal structure, were clearly identified, and no other diffraction peak was observed. This indicates that highly ordered 2D-hexagonal mesoporous structure of SBA-15 has not been altered by the plasma, although SBA-15 and 3%FeO_x/SBA-15 had suffered slight deactivation during the toluene plasma-catalytic oxidation.

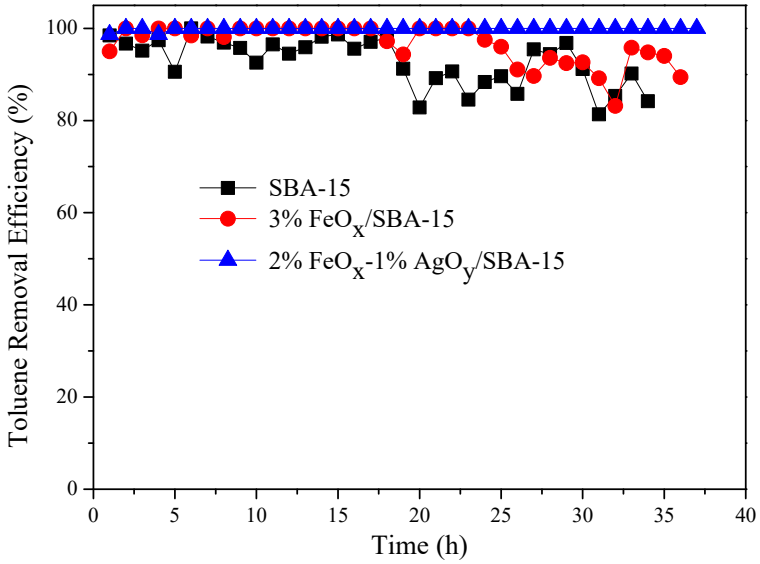

Fig. 9. Toluene removal over different catalysts as a function of time (Initial concentration of toluene: 100 ppm; feed gas: 80%N_2 + 20%O_2).

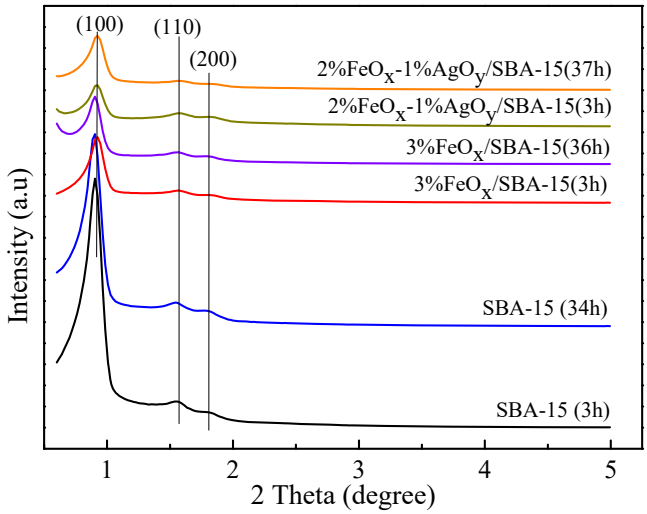

Fig. 10. The low-angle XRD patterns of different catalysts after reaction in plasma at 767 J L^{-1}.

CONCLUSIONS

Combining 3%FeO_x/SBA-15 and 2%FeO_x–1%AgO_y/SBA-15 catalysts with NTP drastically improved their toluene removal efficiency and CO_2 selectivity and markedly reduced the production of organic intermediates. Of these two catalysts, 2%FeO_x–1%AgO_y/SBA-15 exhibited higher CO_2 selectivity and catalyst stability when introduce into nonthermal plasma, which was probably due to the reduced size and the increased dispersion and reducibility of the FeO_x particles following the incorporation of Ag. In addition, Ag, existing in the form of Ag_2O and Ag particles on the catalyst surface, adsorbed toluene and promoted the production of hydroxyl groups, thus improving the reductive activity of the FeO_x. These findings can be used to further optimize the use of FeO_x and AgO_x in plasma-assisted catalyst systems for toluene degradation.

ACKNOWLEDGMENT

This work was supported by the National Natural Science Foundation of China (Grant Nos. 51508245 and 51808269) and the Jiangxi Province Science and Technology Funds for Young Scholars (20192BAB213020). We appreciate Jinbao He, Mr. Rex Howitson for checking the English language. We would also thank the anonymous reviewers for the valuable comments.

REFERENCES

Abdelaziz, A.A., Seto, T., Abdel-Salam, M. and Otani, Y. (2013). Influence of nitrogen excited species on the destruction of naphthalene in nitrogen and air using surface dielectric barrier discharge. *J. Hazard. Mater.* 246–247: 26–33.

Augugliaro, V., Coluccia, S., Loddo, V., Marchese, L., Martra, G., Palmisano, L. and Schiavello, M. (1999). Photocatalytic oxidation of gaseous toluene on anatase TiO_2 catalyst: Mechanistic aspects and FT-IR investigation. *Appl. Catal., B* 20: 15–27.

Blin-Simiand, N., Pasquiers, S., Jorand, F., Postel, C. and Vacher, J. (2009). Removal of formaldehyde in nitrogen and in dry air by a DBD: Importance of temperature and role of nitrogen metastable states. *J. Phys. D: Appl. Phys.* 42: 122003.

Chen, D., Qu, Z.P., Shen, S.J., Li, X.Y., Shi, Y., Wang, Y., Fu, Q. and Wu, J.J.(2011). Comparative studies of silver based catalysts supported on different supports for the oxidation of formaldehyde. *Catal. Today* 175: 338–345.

Chung, W.C., Mei, D.H., Tu, X. and Chang, M.B. (2019). Removal of VOCs from gas streams via plasma and catalysis. *Catal. Rev.* 61: 270–331.

Das, D., Datta, D.B. and Bhattacharya, P. (2014). Simultaneous dyeing and finishing of silk fabric with natural color and itaconic acid. *Clothing Text. Res. J.* 32: 93–106.

Eby, T., Gundusharma, U., Lo, M., Sahagian, K., Marcott, C. and Kjoller, K. (2012). Reverse engineering of polymeric multilayers using AFM-based nanoscale IR spectroscopy and thermal analysis. *Spectrosc. Eur.* 24: 18–21.

Gogoi, P., Nagpure, A.S., Kandasamy, P., Satyanarayana, C. and Thirumalaiswamy, R. (2020). Insights into the catalytic activity of Ru/NaY catalysts for efficient H_2 production through aqueous phase reforming. *Sustainable Energy Fuels* doi: 10.1039/C9SE00797K.

Huang, R., Lu, M.J., Wang, P.T., Chen, Y.D., Wu, J.L., Fu, M.L., Chen, L.M. and Ye,D.Q. (2015). Enhancement of the non-thermal plasma-catalytic system with different zeolites for toluene removal. *RSC Adv.* 5: 72113–72120.

Jiang, N., Hu, J., Li, J., Shang, K.F., Lu, N. and Wu, Y. (2016). Plasma-catalyticdegradation of benzene over Ag–Ce bimetallic oxide catalysts using hybrid surface/packed-bed discharge plasmas. *Appl. Catal., B* 184: 355–363.

Jiang, N., Zhao, Y.H., Qiu, C., Shang, K.F, Lu, N., Li, J., Wu, Y. and Zhang, Y. (2019). Enhanced catalytic performance of CoO_x-CeO_2 for synergetic degradation of toluene in multistage sliding plasma system through response surface methodology (RSM). *Appl. Catal., B* 259: 118061.

Jin, M.S., Kim, J.H., Kim, J.M., Jeon, J.K., Jurng, J., Bae, G.N. and Park, Y.K. (2013). Benzene oxidation with ozone over MnOx/SBA-15 catalysts. *Catal. Today* 204: 108–113.

Li, C.M., Liu, J., Shi, X., Yang, J. and Yang, Q.H (2007). Periodic mesoporous organosilicas with 1, 4-diethylenebenzene in the mesoporous wall: synthesis, characterization, and bioadsorption properties. *J. Phys. Chem. C* 111: 10948–10954.

Li, J.Q., Feng, Y., Mo, S.P., Liu, H., Chen, Y.F. and Yang, J. (2016). NanodendriticPlatinum supported on γ-alumina for complete benzene oxidation. *Part. Part. Syst. Char.* 33: 620–627.

Li, X.Y., Zhu, Z.R., Zhao, Q.D. and Liu, S.M. (2011a). FT-IR study of the photocatalytic degradation of gaseous toluene over UV-irradiated TiO_2 microballs: enhanced performance by hydrothermal treatment in alkaline solution. *Appl. Surf. Sci.* 257: 4709–4714.

Li, X.Y., Zou, X.J., Qu, Z.P., Zhao, Q.D. and Wang, L.Z. (2011b). Photocatalytic degradation of gaseous toluene over Ag-doping TiO_2 nanotube powder prepared by anodization coupled with impregnation method. *Chemosphere* 83: 674–679.

Li, Y.Z., Fan, Z.Y., Shi, J.W., Liu, Z.Y. and Shangguan, W.F. (2014). Post plasma-catalysis for VOCs degradation over different phase structure MnO_2 catalysts. *Chem. Eng. J.* 24: 251–258.

Liang, W.J., Ma, L., Liu, H. and Li, J. (2013). Toluene degradation by non-thermal plasma combined with a ferroelectric catalyst. *Chemosphere* 92: 1390–1395.

Long, L.P., Zhao, J.G., Yang, L.X., Fu, M.L., Wu, J.L., Huang, B.C. and Ye, D.Q. (2011). Room temperature catalytic ozonation of toluene over MnO_2/Al_2O_3. *Chinese J. Catal.* 32: 904–916. (in Chinese)

Lu, M., Huang, R., Wu, J., Fu, M., Chen, L. and Ye, D. (2015). On the performance and mechanisms of toluene removal by FeOx/SBA-15-assisted non-thermal plasma at atmospheric pressure and room temperature. *Catal. Today* 242: 274–286.

Lu, M.J, Huang, R., Wang, P.T., Chen, L.M., Wu, J.L., Fu, M.L., Wen, W., Huang,B.C. and Ye, D.Q. (2014). Plasma-catalytic oxidation of toluene on Mn_xO_y at atmospheric pressure and room temperature. *Plasma Chem. Plasma Process.* 34: 1141–1156.

Lu, W.J., Abbas, Y.W., Mustafa, M.F., Pan, C. and Wang, H.T. (2019). A review on application of dielectric barrier discharge plasma technology on the abatement of volatile organic compounds. *Front. Environ. Sci. Eng.* 13: 30.

Maira, A., Coronado, J., Augugliaro, V., Yeung, K., Conesa, J. and Soria, J. (2001). Fourier Transform Infrared Study of the Performance of Nanostructured TiO_2 Particles for the Photocatalytic Oxidation of Gaseous Toluene. *J. Catal.* 202: 413–420.

Pangilinan, C. D. C., Kurniawan, W., Salim, C. and Hinode, H. (2016). Effect of Ag/TiO_2 catalyst preparation on gas-phase benzene decomposition using non-thermal plasma driven catalysis under oxygen plasma. *React. Kinet. Mech. Catal.* 117: 103–118.

Qin, C.H., Dang, X.Q., Huang, J.Y., Teng, J.J. and Huang, X.M. (2016). Plasma-catalytic oxidation of adsorbed toluene on Ag–Mn/γ-Al_2O_3: Comparison of gas flow-through and gas circulation treatment. *Chem. Eng. J.* 299: 85–92.

Qin, Y., Qu, Z.P., Dong, C., Wang, Y. and Huang, N. (2019). Highly catalytic activity of Mn/SBA-15 catalysts for toluene combustion improved by adjusting the morphology of supports. *J. Environ. Sci.* 76: 208–216.

Scirè, S., Minicò, S., Crisafulli, C. and Galvagno, S. (2001). Catalytic combustion of volatile organic compounds over group IB metal catalysts on Fe_2O_3. *Catal. Commun.* 2: 229–232.

Stasiulaitiene, I., Martuzevicius, D., Abromaitis, V., Tichonovas, M., Baltrusaitis, J., Brandenburg, R.,

Pawelec, A. and Schwock, A. (2016). Comparative life cycle assessment of plasma-based and traditional exhaust gas treatment technologies. *J. Cleaner Prod.* 112: 1804–1812.

Trinh, Q. H., Lee, S. B. and Mok, Y. S. (2015). Removal of ethylene from air stream by adsorption and plasma-catalytic oxidation using silver-based bimetallic catalysts supported on zeolite. *J. Hazard. Mater.* 285: 525–534.

Wang, W.Z., Wang, H.L., Zhu, T. L.and Fan, X. (2015). Removal of gas phase low-concentration toluene over Mn, Ag and Ce modified HZSM-5 catalysts by periodical operation of adsorption and non-thermal plasma regeneration. *J. Hazard. Mater.* 292: 70–78.

Yang, H.G., Deng, J.G., Liu, Y.X., Xie, S.H., Wu, Z.X. and Dai, H.X. (2016). Preparation and catalytic performance of Ag, Au, Pd or Pt nanoparticles supported on 3DOM CeO_2–Al_2O_3 for toluene oxidation. *J. Mol. Catal. A: Chem.* 414: 9–18.

Yang, Y., Zhang, W., Wu, J.L., Fu, M.L., Chen, L.M. and Huang, B.C. (2013). In situ infrared spectroscopic studies of plasma-catalytic degradation of toluene. *Acta Sci. Circumst.* 33: 3138–3145. (in Chinese)

Yu, L., Tu, X., Li, X.D., Wang, Y., Chi, Y. and Yan, J.H. (2010). Destruction of acenaphthene, fluorene, anthracene and pyrene by a dc gliding arc plasma reactor. *J. Hazard. Mater.* 180: 449–455.

Zhang, H.L., Tang, C.J., Sun, C.Z., Qi, L., Gao, F., Dong, L. and Chen, Y. (2012a). Direct synthesis, characterization and catalytic performance of bimetallic Fe–Mo-SBA-15 materials in selective catalytic reduction of NO with NH_3. *Microporous Mesoporous Mater.* 151: 44–55.

Zhang, W.W., Qu, Z.P., Li, X.Y., Wang, Y., Ma, D. and Wu, J.J. (2012b). Comparison of dynamic adsorption/desorption characteristics of toluene on different porous materials. *J. Environ. Sci.* 24: 520–528.

Zhang, X.D., Qu, Z.P., Yu, F.L. and Wang, Y. (2013). High-temperature diffusion induced high activity of SBA-15 supported Ag particles for low temperature CO oxidation at room temperature. *J. Catal.* 297: 264–271.

Zhu, X.B., Liu, S.Y., Cai, Y.X., Gao, X., Zhou, J.S., Zheng, C.H. and Tu, X. (2016). Post-plasma catalytic removal of methanol over Mn–Ce catalysts in an atmospheric dielectric barrier discharge. *Appl. Catal., B* 183: 124–132.

Received for review, September 18, 2019
Revised, November 29, 2019
Accepted, November 30, 2019